Title: Probe-Assisted Detection of Fe³⁺ Ions in a Multi-Functionalized Nanopore

Author: Pearl Arora^a, Haiyan Zheng^b, Sathishkumar Munusamy^b, Rana Jahani^b, Liang Wang^{c,d,*}, and Xiyun Guan^{b,*}

Author affiliation:

^aDepartment of Chemistry, Illinois Institute of Technology, Chicago, IL 60616, USA

^bDepartment of Chemistry, University of Missouri, Columbia, MO 65211, USA

^cChongqing Institute of Green and Intelligent Technology, Chinese Academy of Sciences, Chongqing 400714, China

^dChongqing School, University of Chinese Academy of Sciences, Chongqing 400714, China

^{*}Corresponding Authors e-mails: wangliang83@cigit.ac.cn; and xgpc2@missouri.edu.

Probe-Assisted Detection of Fe³⁺ Ions in a Multi-Functionalized

Nanopore

Abstract

Iron is an essential element that plays critical roles in many biological/metabolic processes, ranging from oxygen transport, mitochondrial respiration, to host defense and cell signaling. Maintaining an appropriate iron level in the body is vital to the human health. Iron deficiency or overload can cause life-threatening conditions. Thus, developing a new, rapid, cost-effective, and easy to use method for iron detection is significant not only for environmental monitoring but also for disease prevention. In this study, we report an innovative Fe³⁺ detection strategy by using both a ligand probe and an engineered nanopore with two binding sites. In our design, one binding site of the nanopore has a strong interaction with the ligand probe, while the other is more selective toward interfering species. Based on the difference in the number of ligand DTPMPA events in the absence and presence of ferric ions, micromolar concentrations of Fe³⁺ could be detected within minutes. Our method is selective: micromolar concentrations of Mg²⁺, Ca²⁺, Cd²⁺, Zn²⁺, Ni²⁺, Co²⁺, Mn²⁺, and Cu²⁺ would not interfere with the detection of ferric ions. Furthermore, Cu²⁺, Ni²⁺, Co²⁺, Zn²⁺, and Mn²⁺ produced current blockage events with quite different signatures from each other, enabling their simultaneous detection. In addition, simulated water and serum samples were successfully analyzed. The nanopore sensing strategy developed in this work should find useful application in the development of stochastic sensors for other substances, especially in situations where multi-analyte concurrent detection is desired.

Keywords: Multi-functionalized nanopore; Molecular probe; Ferric ions; Multi-analyte simultaneous detection; Single-molecule sensor

Introduction

Iron is one such element that is plentiful and crucial in nature. Particularly in humans where ~70% iron is stored in the form of hemoglobin in blood and as myoglobin in muscle, many biological processes depend on iron as a cofactor (Chakraborty et al., 2020). It possesses a unique property of being an electron donor as well as acceptor, and hence plays important roles in many biological/metabolic processes (e.g., carrying out electron transport reactions, transferring of oxygen, and DNA synthesis) (Boldt, 1999). Accordingly, maintaining an appropriate iron level in the body is vital to the human health. Iron deficiency or overload can cause life-threatening conditions. For example, when there is not enough iron in the body, iron deficiency anemia can develop. Furthermore, iron deficiency can lead to poor oxygen transfer to cells, liver problems, diabetes, etc. On the other hand, hemochromatosis is an iron overload disease. Excess iron can build up in organs such as liver, heart, and endocrine glands and cause damage. It has also been reported that iron overload can cause Alzheimer's, Huntington's and Parkinson's diseases through the formation of free radicals (Harigae, 2018). Accordingly, determination of total serum iron concentration and total iron binding capacity test have been useful methods in disease diagnosis such as anemia and hemochromatosis in clinical settings (Hirayama and Nagasawa, 2017). It should be noted that iron can enter environmental water bodies through many ways such as metal mining, industrial waste dumping, oxidation of water pipelines and as raw material for manufacturing purposes. The imbalance of iron levels in environmental water bodies can negatively impact the marine ecosystem. Since serious health problems can occur in humans due to uncontrolled and excessive intake of iron in the body, the US Environmental Protection Agency (EPA) has set the maximum allowance level of 5.4 µM for Fe³⁺ ions in drinking water. Thus far, several analytical techniques have been developed for Fe³⁺ detection, including fluorescence-based (Cui et al., 2019; Liu et al., 2022; Shellaiah et al., 2020; Ye et al., 2022); electrochemical (Bansod et al., 2017; Laglera and Monticelli, 2017; Wu et al., 2023; Zhu et al., 2017), inductively coupled plasma mass spectrometry (ICP-MS) (Qin et al., 2021; Shariff et al., 2018; Yu et al., 2020) and atomic spectroscopy (dos Santos et al., 2022; Paz-Rodríguez et al., 2015). However, most of these methods require the use of expensive and complex instruments, and/or involve extensive sample preparation and are time consuming. Therefore, there is a need for the development of a new, rapid, cost-effective, and easy to use method for detection of iron in clinical, environmental and industrial samples.

Nanopore sensing has gained increasing interest due to its advantages of label-free and single molecule analysis. When an analyte passes through a nano-scale sized channel under a fixed potential bias, it undergoes transitory interactions (e.g., electrostatic, H-bonding, aromatic, etc.) with the inner walls of nanopore, resulting in ionic current modulations (events). As each event corresponds to the direct sensing of a single molecule passing through the channel, nanopore technique provides important information such as size, charge, and concentration of the analyte. Over the last two decades, nanopore has been used as a versatile tool for various applications. These include enantiomeric discrimination (Kang et al., 2006), studying covalent and noncovalent interactions (Chen et al., 2021), probing enzymatic activity and kinetics (Zhou et al. 2016), and biosensing of numerous species such as DNA (Kececi et al., 2022; Li et al., 2021; Lu et al., 2015; Wang et al., 2018), RNA (Lee et al., 2021; Rozevsky et al., 2020; Zhang et al., 2022), proteins (Ahmad et al., 2023; Hu et al., 2021; Zhang et al., 2020), polymers (Singh et al., 2023), heavy and/or radioactive metals (Roozbahani et al., 2018, 2017; Song et al., 2023; Vaneev et al., 2023), and toxic substances (Han et al., 2015; L. Wang et al., 2014). In particular, in terms of metal ion detection, three major strategies have been developed, including (i) creating metal ion binding sites in the inner surface of the nanopore (Bayley et al., 2000; Cao et al., 2019; X. Chen et al., 2021; Choi et al., 2013; Zhan et al., 2020); (ii) utilization of a ligand probe (Roozbahani et al., 2018, 2017; G. Wang et al., 2014; Wang et al., 2013, 2016, 2017; Wei et al., 2018); and iii) taking advantage of enzymatic reactions (Liu et al., 2016; Roozbahani et al., 2019; Zhou et al., 2016). An excellent review regarding nanopore-based metal ion detection has been written by Roozbahani and co-workers recently (Roozbahani et al., 2020). In this work, we are demonstrating a new strategy for metal ion detection by using both a ligand probe and an engineered nanopore with two binding sites to improve the sensor selectivity and enable multi-analyte concurrent quantification. Our developed nanopore sensing strategy should have potential application in monitoring Fe³⁺ in real world samples such as running water, lake water, and even in biological fluids such as human serum.

Experimental Section

1.1. Materials and Reagents

DTPMPA (short for Diethylenetriaminepenta(methylene-phosphonic acid)), NaCl, HCl (ACS reagent, ≤1 ppm heavy metals), NaH₂PO₄ (BioXtra grade, 99.5%), Trizma base (BioXtra grade, ≥99.5%), Fe(NO₃)₂, CaCl₂, Ni(NO₃)₂, Co(NO₃)₂, Cd(NO₃)₂, Mg(NO₃)₂, Cu(NO₃)₂, Zn(NO₃)₂, Mn(NO₃)₂, and human serum (from human male AB plasma, USA origin) were purchased from Sigma-Aldrich (St. Louis, MO). All the stock solutions, including those of the metal salts as well as the ligand DTPMPA, were prepared at 10 mM each using HPLC-grade water. The buffer solution used for nanopore experiments contained 1 M NaCl and 10 mM Tris with the solution pH adjusted to 7.5 with HCl. The phosphatidylcholine-1,2-diphosphocholine lipid was bought from Avanti Polar Lipids (Alabaster, AL). Teflon film was ordered from Goodfellow (Malvern, PA), and the engineered His-tagged α-hemolysin (α-HL) (M113K)₇ protein was synthesized according to a protocol described previously (Han et al., 2015; Zhao et al., 2008).

1.2. Single-channel Recording Experiments

A vertical chamber set-up was used to carry out single-channel recordings. Briefly, two compartments, *cis* and *trans*, were created with a Teflon film as the septum, and a DPhPC bilayer was produced over a 120-150 μm opening in the film using the Montal-Mueller technique (Montal and Mueller, 1972). The solutions in the compartments consisted of 1 M NaCl buffered with 10 mM Tris at pH 7.5. In the *cis* compartment, which was connected to "ground," α-HL proteins and DTPMPA were introduced. The final α-HL protein concentration for single-channel insertion was 0.05-0.2 ng/mL. Using a patch-clamp amplifier (Axopatch 200B, Molecular Devices, Sunnyvale, CA), we were able to capture ionic currents that were filtered at 5 kHz by an integrated four-pole Bessel filler and sampled at 20 kHz by a computer connected with a Digidata 1440A A/D converter (Molecular Devices).

1.3. Data Analysis

Clampfit 10.7 (Molecular Devices) software was used to obtain the amplitude and duration of the single-channel blockage events. Briefly, the event mean residence time (τ_{off}) was calculated from the dwell histogram by fitting with a single exponential function. To derive the blockage amplitude, a Gaussian function is used to fit the amplitude histogram. The results of Fe³⁺ detection in this study are reported in the form of percent reduction of DTPMPA events, which is calculated using the equation: $\Delta n / n_0 = (n_0 - n_1) / n_0$, where n_0 and n_1 represented the number of DTPMPA events in absence and presence of metal ions. Each single channel recording experiment was run

for a minimum of 10 minutes. For each sample testing, experiments were conducted at least three times with a fresh protein nanopore employed.

2. Results and Discussion

2.1. Probe Selection and Sensing Element

As documented in the literature (Roozbahani et al., 2018, 2017; Wei et al., 2018), direct detection of metal ions based on their translocation in a nanopore is challenging due to their rapid translocation, the incompatible size/dimension between them and the nano-channel, and the resolution of the nanopore sensing equipment. To sensitively detect ferric ions, DTPMPA (short for diethylenetriamine penta(methylene phosphonic acid), Fig. 1a) was used as a chelating probe in our investigation. DTPMPA molecules are hard bases due to the presence of plenty of amine N and phosphonate O atoms, while iron ions are hard acids. According to the soft and hard acid-base principle, iron ions can easily combine with O and N (Mady et al., 2021). Moreover, DTPMPA (in salt form) is water-soluble, which makes it a good ligand probe used for nanopore analysis. Unfortunately, although DTPMPA is a bulky molecule, its translocation in the wild-type αhemolysin (α -HL) nanopore rarely produced observable current modulation events due to the strong electrophoretic force exerted on DTPMPA as well as the weak interaction between DTPMPA and the nanopore. Note that α-HL protein is the most widely used stochastic sensing element in the nanopore field, which has an opening of approximately 2.6 nm in diameter and a constriction of about 1.4 nm in diameter (Song et al., 1996). To slow the translocation of DTPMPA in the nanopore, a functionalized α-HL nanopore, namely M113K, was designed and utilized as the sensing element in this study. In the produced M113K protein pore, the methionine residues at position 113 of the wild-type α -HL were replaced by lysine amino acids. The presence of 7 lysine residues near the constriction of the α-HL pore makes it anion selective (Gupta et al., 2013), thus enhancing the resolution of the nanopore toward detection of DTPMPA (which is a negatively charged species). However, due to its polydentate ligand property, DTPMPA can potentially interact with many other metal ions, thus interfering with the detection of the target Fe³⁺ ions. To minimize the potential interference from other metal ions, we further engineered this protein pore with 6 histidine tags at position 293, which is close to the cis entrance of the channel (Fig. 1b). It is well known that histidine residues possess strong affinity towards divalent metals such as Cu²⁺,

Ni²⁺, Co²⁺, and Zn²⁺ due to the strong chelation interactions (Liu et al., 2016; Minicozzi et al., 2008; Roozbahani et al., 2017; Wang et al., 2020). Thus, the combined use of the DTPMPA ligand probe and His-tagged M113K protein provided an effective method for the detection of Fe³⁺ in aqueous solutions with high sensitivity and selectivity. Taken together, our sensing system is designed in such a manner that the competitive interaction between the ligand probe DTPMPA and Fe³⁺ as well as the lysine residues introduced into the α -HL pore determines the sensor sensitivity, while the relative binding affinities of Fe³⁺ versus other metal ions toward DTPMPA and the histidine residues located in the mushroom cap of α -HL play important roles in the sensor selectivity.

The strategy for nanopore detection of Fe³⁺ is shown in Fig. 1c. In the absence of metal ions, the translocation of the ligand probe DTPMPA through the nanopore produced current blockage events with large amplitude and long residence time due to its large molecular size and its strong interaction with the lysine residues (i.e., the recognition site) introduced in the engineered nanochannel. In contrast, in the presence of Fe³⁺ ions, new events with shorter dwell time and smaller blockage amplitude will appear, accompanied by a significant reduction in the frequency of the ligand DTPMPA events. The short-lived events are attributed to the formation of metal-DTPMPA complex as the complex carries considerably lesser negative charge than uncomplexed DTPMPA molecule, thus leading to a weaker interaction with the recognition site.

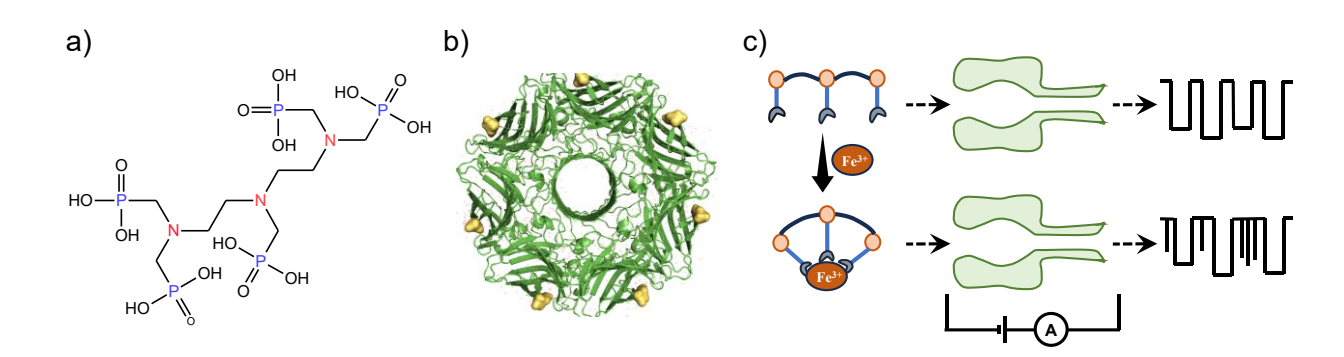
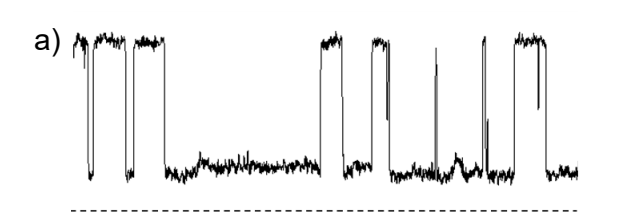
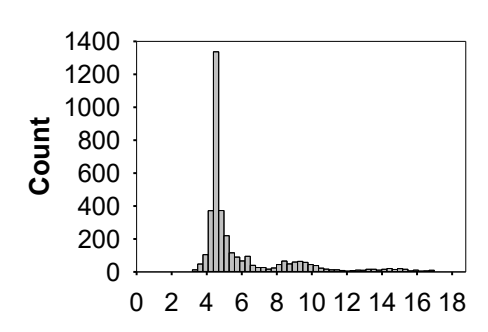


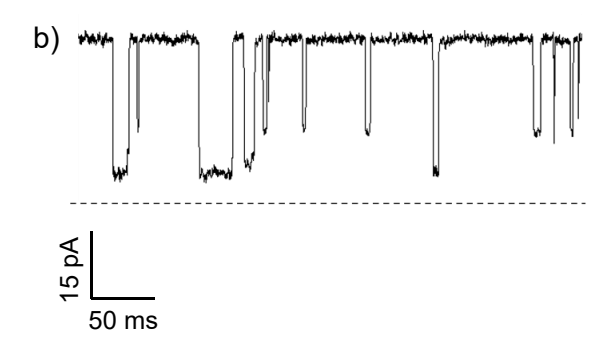
Figure 1. Nanopore sensing of Fe³⁺ with DTPMPA and a His-tagged α-HL M113K protein pore. Structures of a) DTPMPA and b) His-tagged M113K α-HL protein pore with the His-tag positions highlighted as gold colored spheres; and c) Schematic representation of the principle of Fe³⁺ detection. DTPMPA alone in the nanopore generated one major type of long-lived events. However, in the presence of Fe³⁺, in addition to a decrease in the frequency of the ligand DTPMPA events, a new type of events (attributed to the DTPMPA-Fe³⁺complex) with different dwell time were produced.

2.2. Detection of Fe³⁺ ions using DTPMPA probe

To examine the viability of utilizing our designed nanopore sensing strategy for Fe³⁺ detection, initial experiments were carried out at +40 mV under symmetric electrolyte conditions with 1 M NaCl and 10 mM Tris (pH 7.5) in the His-tagged α-HL M113K protein pore (note that this engineered protein was able to function properly at other experimental conditions such as high salt, salt gradient, acidic and basic solutions, Figs. S1-S5). As shown in Figure 2, in the absence of Fe³⁺, the interaction of DTPMPA (which was added to the *cis* side of the sensing chamber) with the α-HL nanopore produced one major type of current blockage events with a mean residual current of 4.5 ± 1.2 pA and residence time of 31.2 ± 4.9 ms. The appearance of large blockage amplitude and long dwell time events are reasonable because DTPMPA is a bulky molecule bearing negative charge, so that it would experience strong electrostatic interaction with the positively charged binding sites located in the M113K protein nanopore, leading to long-duration blockage of the flux of ions transferring through the nano-channel. In contrast, after addition of Fe³⁺ ions to the solution, we observed a striking decrease in the number of DTPMPA events, while a new type of events with shorter residence time (3.2 \pm 0.5 ms) and larger residual current (14.3 \pm 0.8 pA) appeared (Figure 2b). Clearly, the new type of events was attributed to the produced Fe³⁺-DTPMPA complex. Compared with free DTPMPA, the Fe³⁺- DTPMPA complex molecules carry less negative charges, resulting in weaker interaction with the M113K protein nanopore. The quite different event residence time and blockage amplitude allowed for convenient separation of free DTPMPA from Fe³⁺-DTPMPA complexes. In addition, about 50% reduction in the frequency of DTPMPA events was observed after addition of Fe³⁺ ions to the DTPMPA-containing solution, further supporting the fact that the ligand was involved in complex formation when ferric ions were present.







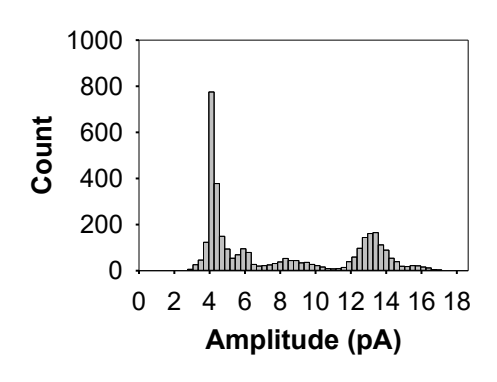


Figure 2. Nanopore detection of Fe³⁺ ions using ligand DTPMPA. (a) 10 μM DTPMPA; and (b) 10 μM DTPMPA + 20 μM Fe³⁺. (*Left*) Typical single-channel current recording trace segments; and (*Right*) the corresponding event amplitude histograms. The experiments were performed at +40 mV with the Histagged (M113K)₇ αHL pore in an electrolyte solution containing 1.0 M NaCl and 10 mM Tris (pH 7.5). Both DTPMPA and ferric ions were added to the *cis* compartment of the nanopore sensing chamber. Dashed lines represent the levels of zero current.

2.3. Effects of voltage bias and DTPMPA concentration on ferric ion detection

To determine an appropriate experimental condition on nanopore detection of Fe³⁺, we next investigated the translocation of DTPMPA in the nanopore at varying voltages in the presence and the absence of metal ions. Our study (Fig. 3) revealed that, with an increase in the applied potential bias from +20 mV to +60 mV, the event blockage residual current of both the ligand DTPMPA and the metal-ligand complex increased almost four times (from 2.4 ± 0.2 pA to 9.4 ± 0.9 pA, and from 6.7 ± 0.3 pA to 24.0 ± 1.5 pA, respectively). In contrast, the event frequency of both the two species increased with the voltage until reaching +50 mV (from 1.9 ± 0.3 to 28.5 ± 2.0 and from 2.0 ± 1.0 to 20.9 ± 1.9 , respectively) and then decreased significantly at higher applied potentials. It is likely that, at a voltage bias larger than +50 mV, DTPMPA and its metal complex translocated through the nanopore too rapidly, so that many of their events could not be captured by the nanopore sensing instrument. Further data analysis showed that, the residence time of free DTPMPA decreased significantly (from 455.2 ± 6.0 ms to 0.85 ± 0.09 ms) as the applied voltage increased from +20 mV to +60 mV, and a similar approx. 97% reduction in the dwell time of DTPMPA- Fe³⁺ complex was observed. This observation is not unreasonable considering that our nanopore sensing strategy is based on a combination of electrostatic interaction and electrophoretic effect (note again that DTPMPA is a negatively charged species). Clearly, if we increase the applied potential bias, there would be more flux of ions passing through the channel and hence more events will be produced, meanwhile reducing the time that analyte molecules stay in the pore. A potential of +40 mV was chosen as the optimum voltage for the remaining experiments because although a larger event frequency was obtained at +50 mV, the resolution to differentiation between the DTPMPA events and the metal-ligand complex events decreased, making data analysis difficult and less accurate.

At the optimum applied potential (i.e., + 40 mV), the plot of the event frequency as a function of the ligand DTPMPA concentration was further investigated. Our experimental results (Fig. 3d)

showed that the event frequency of DTPMPA increased linearly with increasing DTPMA concentration until it reached $\sim 4~\mu M$, suggesting that the sensitivity of the nanopore sensor would not differ significantly as long as the concentration of DTPMPA was not too large (more than 4 μM). A concentration of 2 μM DTPMPA was chosen as the optimum ligand concentration and used in the remaining experiments, as it could yield enough events with a good signal to noise ratio required for data analysis within relatively short period of time.

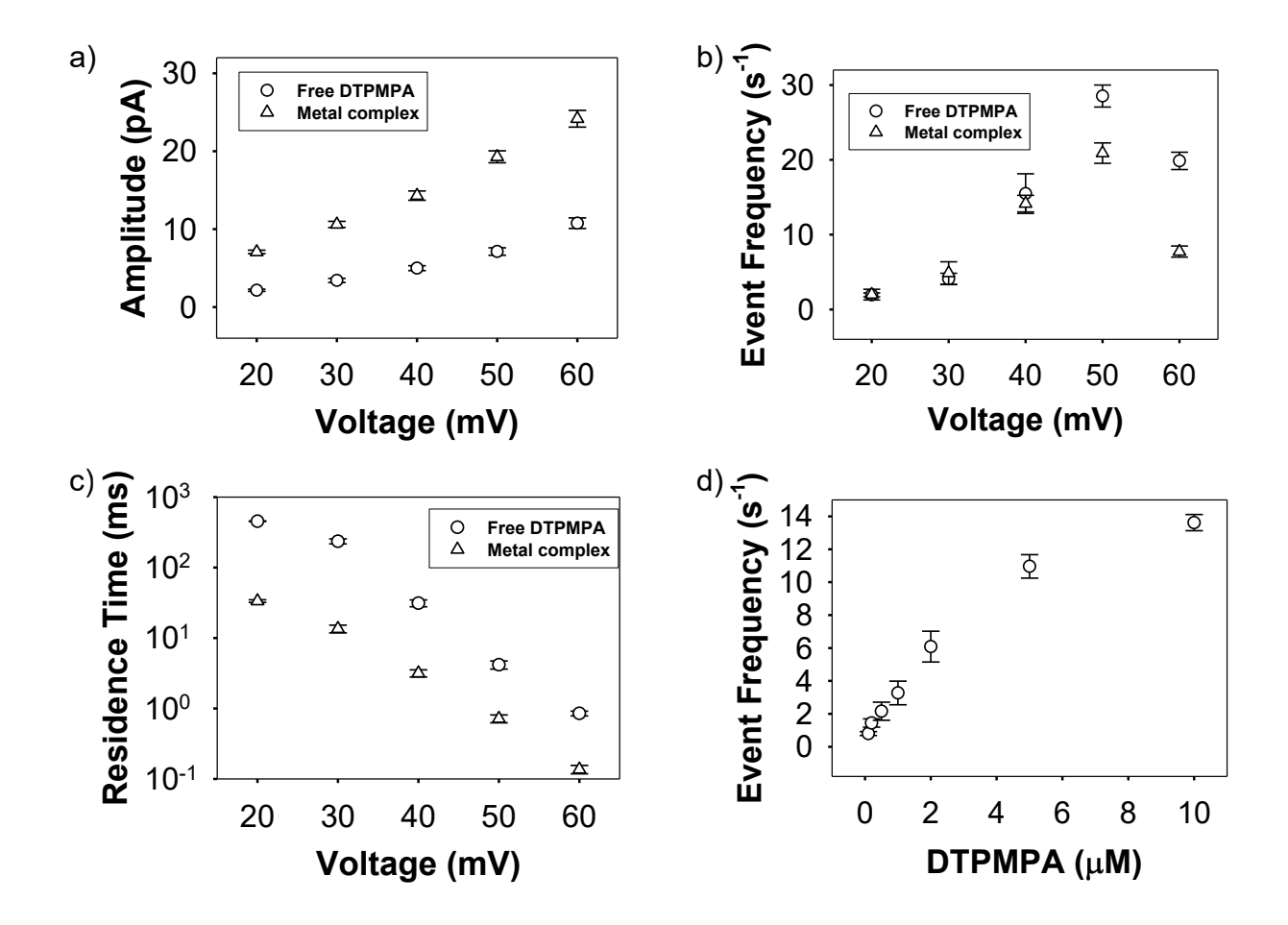


Figure 3. The effect of the applied potential bias on the (a) blockage amplitude; (b) event frequency; and (c) residence time. Experiments were performed with the His-tagged (M113K)₇ α HL protein nanopore in an electrolyte solution containing 1 M NaCl and 10 mM Tris (pH 7.5) and in the presence of 10 μ M DTPMPA and 20 μ M Fe³⁺ at various voltages ranging from +20 mV to +60 mV. d) The plot of the event frequency versus DTPMPA concentration. These experiments were performed at +40 mV with the His-tagged (M113K)₇ α HL nanopore.

2.4. Sensitivity and Selectivity

With a fixed DTPMPA concentration at 2 µM and at a + 40 mV applied potential bias, the effect of Fe³⁺ ions concentration on the interaction between nanopore and DTPMPA was studied. The dose-response curve for Fe³⁺ detection was constructed by plotting the percent reduction in the number of DTPMPA events vs. Fe3+ concentration. We found out that there was a linear relationship between them (up to $\sim 10 \mu M$ of Fe³⁺). The limit of detection (LOD) for this system in a 10-minute recording was $0.28~\mu M$ (LOD is defined as the Fe^{3+} concentration yielding a signal equal to the mean of the blank signal plus three times the standard deviation of blank divided by the slope of the calibration curve). Such a detection limit, although not as impressive as those of electrochemical methods, is as good as those of other various sensitive Fe³⁺ detection methods developed thus far (Table S1). It is worth mentioning that iron is an abundant essential element for virtually all living organisms. It is not only present in the human body and environment, but also a widely used raw material for industry. Regular iron detection to prevent iron imbalance is highly important. Our developed nanopore sensor is sensitive enough for analyzing Fe³⁺ in clinical, environmental and industrial samples (note that the maximum limit of Fe³⁺ ions in drinking water set by the U.S. Environmental Protection Agency is 5.4 µM). Further improvement in the sensor sensitivity might be achieved by using a lower concentration of the ligand DTPMPA or changing the experimental conditions. For example, using high salt, employing an asymmetric electrolyte gradient instead of the conventional symmetric electrolyte buffer, and varying the pH of the electrolyte solution are well-established strategies to improve the sensitivity and resolution of the nanopore sensor (Chen et al., 2018; de Zoysa et al., 2011; Roozbahani et al., 2017; Wang et al., 2014; Wanunu et al., 2010; Zhao et al., 2008). These studies are currently under way in out laboratory (Figs. S1-S5).

To assess the selectivity of the Fe³⁺ nanopore sensor, eight metal ions with comparable chemical characteristics and/or distributions in natural water were selected as potential interfering species, including Ca²⁺, Mg²⁺, Zn²⁺, Ni²⁺, Co²⁺, Cu²⁺, Cd²⁺, and Mn²⁺. The effects of these eight metal ions on the translocation of DTPMPA in the engineered α -HL nanopore were investigated using the same experimental conditions as used in the Fe³⁺ dose-response study. Our experiments suggested that the presence of these metal ions in the solution would not have a significant impact on ferric ion detection although they indeed interacted with the ligand, forming complexes. To be more specific, based on the responses of the nanopore sensor toward the eight cationic species, they can be divided into two major categories. Similar to Fe³⁺, addition of Mg²⁺ and Cd²⁺ ions to

the solution did not affect the blockage amplitude and residence time of DTPMPA in the nanopore but resulted in a decrease in its event frequency. On the contrary, presence of Ca²⁺ in the solution led to an increase in the frequency of DTPMPA events (Fig. 4b), which might be attributed to the salt effect. Nevertheless, even at concentrations of 5 µM, these divalent metal ions only caused small event count changes (~3% for Mg²⁺, ~10% for Ca²⁺, and ~11% for Cd²⁺, respectively). Hence, their interfering effect is negligible, as a $\sim 48\%$ decrease in the number of DTPMPA events was observed after addition of Fe³⁺. On the other hand, if the solution contained Ni²⁺, Co²⁺, Cu²⁺, Zn²⁺, or Mn²⁺, DTPMPA produced current modulation events with quite different blockage amplitudes and residence time from those of DTPMPA alone or in the presence of Fe³⁺. For example, as shown in Fig. 4c, the blockage residual current of DTPMPA in the presence of Ni²⁺, Co^{2+} , and Zn^{2+} was 6.95 ± 1.2 pA, 6.54 ± 1.8 pA, and 5.3 ± 0.4 pA, respectively, which can be differentiated from those of Fe³⁺ (4.5 \pm 0.1 pA). Most strikingly, in the presence of Mn²⁺ or Cu²⁺ ions, DTPMPA events showed sub-state current levels, which set Mn²⁺ and Cu²⁺ apart from all the other metal ions. Additionally, the dwell time values of DTPMPA events in the presence of Ni²⁺ $(6.9 \pm 0.3 \text{ ms})$, Zn^{2+} $(23.6 \pm 4.5 \text{ ms})$, Mn^{2+} $(44.1 \pm 0.1 \text{ ms})$, and Co^{2+} $(91.3 \pm 3.4 \text{ ms})$ were quite different, allowing these four metal species readily differentiated. The significantly different responses of the nanopore sensor toward two categories of metal ions (i.e., Ca²⁺, Mg²⁺, Cd²⁺, and Fe³⁺ vs. Zn²⁺, Ni²⁺, Co²⁺, Cu²⁺, and Mn²⁺) suggests that the His-tags near the mushroom cap of the nanopore played a significant role in the sensor selectivity, which is in agreement with the fact that His-tags are well-known ligands for Cu²⁺, Ni²⁺, Co²⁺ and Zn²⁺ (Wang et al., 2020). To gain more insight into the mechanism of this sensing system, the interactions between the nanopore and Cu²⁺ / Ni²⁺ were further investigated. Our experimental results showed that Cu²⁺ or Ni²⁺ alone in the nanopore didn't produce any observable current modulation events. Furthermore, the open channel current did not change before and after addition of Cu²⁺ or Ni²⁺ (Figs. S6 and S7), indicating that the metal/His-tags interaction would not cause a size change in the β-barrel of the nanopore (note that the β-barrel determines the open channel current since it has a much smaller dimension than the mushroom cap and lumen of the nanopore). Therefore, it is likely that the interactions between the His-tags and Zn²⁺, Ni²⁺, Co²⁺, Cu²⁺, or Mn²⁺ might result in slight conformational changes in the nanopore lumen, which would then impact the translocation of DTPMPA molecules through the nanopore, thus producing events with different signatures. Taking together, although DTPMPA is not a highly specific chelating agent, its larger binding affinity with Fe³⁺ versus many other metal ions and the interactions between the histidine tags and interfering metals as well as the possibly induced conformational changes in the nanopore lumen not only make the nanopore sensor more selective to Fe³⁺, but also enable potential simultaneous detection of Ni²⁺, Co²⁺, Cu²⁺, Zn²⁺, and Mn²⁺.

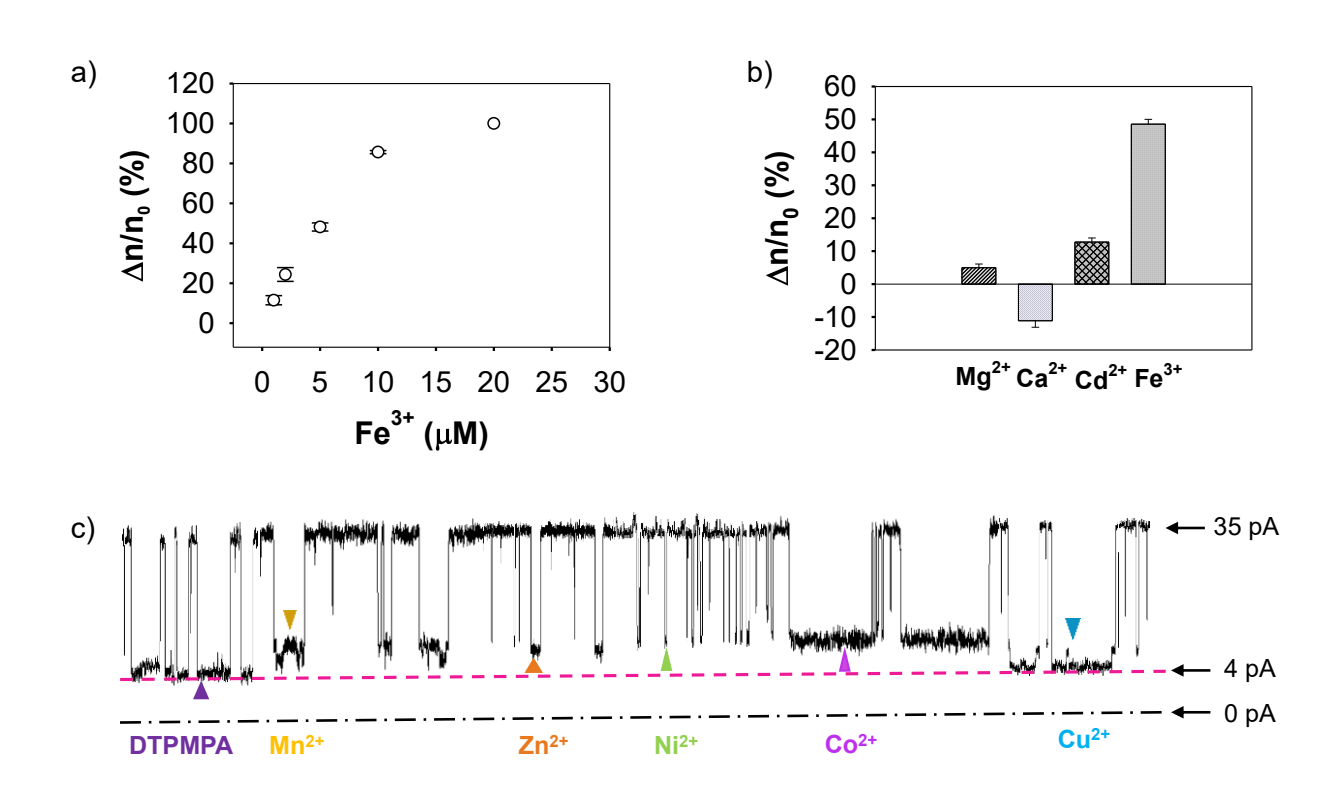


Figure 4. Sensitivity and selectivity of the Fe³⁺ nanopore sensor. (a) Dose—response curve; (b) Interference study; and c) Superimposed single-channel current trace for DTPMPA alone, DTPMPA-Zn²⁺, DTMPA-Ni²⁺, DTPMPA-Co²⁺, DTMPA-Mn²⁺, and DTPMPA-Cu²⁺. The experiments were performed at +40 mV with the His-tagged (M113K)₇ α-HL protein nanopore in an electrolyte solution containing 1 M NaCl and 10 mM Tris•HCl (pH 7.5) and in the presence of 2 μM DTPMPA. The concentrations of the metal ions shown in parts b and c were 5 μM each. In parts a and b, the change in the number of DTPMPA events after addition of Fe³⁺ or other metal ions to the solution was calculated by using the equation $\Delta n = (n_0 - n_1)/n_0$, where n_0 represented the number of DTPMPA events in the absence of metal ions, while n_1 depicted the number of DTPMPA events in the presence of metal ions. In part c, the colored triangle symbols indicate the DTPMPA events in the absence and presence of Zn²⁺, Ni²⁺, Co²⁺, Mn²⁺, and Cu²⁺ ions, suggesting that Fe³⁺, Ni²⁺, Co²⁺, Mn²⁺, Cu²⁺ and Zn²⁺ could be readily differentiated by our constructed nanopore sensor and even achieved simultaneous detection.

2.5. Simulated Water and Human Serum Sample Analysis

Three simulated water samples and one mock human serum sample were used to examine the efficacy of our nanopore sensor in real-world applications. Briefly, 5 µM ferric ions were spiked into tap water from our life science building, lake water from Lake Michigan, Kirkland brand bottled spring water and human serum (Sigma-Aldrich), respectively, and then analyzed by our constructed nanopore sensor. The experimental results are summarized in Table 1. From the table, we could see that the recoveries (ranging from 96 % to 129 %) of Fe³⁺ from the water and serum samples determined by use of the nanopore sensor were satisfactory, indicating that the matrix component in the water and serum would not greatly affect ferric ion detection, and our developed Fe³⁺ sensing platform has a potential application in the analysis of real-world samples.

Table 1. Recovery of Fe³⁺ ions from water and serum samples by use of the nanopore stochastic sensing method. Each experimental value represents the mean of three replicate analyses \pm one standard deviation.

Sample Type	Theoretical Value (μM)	Experimental Value (µM)
Tap water	5.00	5.61 ± 0.08
Bottle water	5.00	5.11 ± 0.20
Lake water	5.00	4.78 ± 0.26
Human serum	5.00	6.44 ± 0.34

3. Conclusion

In summary, a selective and sensitive stochastic sensor was successfully developed to detect Fe³⁺ ions by combined use of a ligand probe and an engineered nanopore with two binding sites. In our nanopore sensor design, the competitive interactions among the metal ions, the chelating agent (i.e., DTPMPA) and the lysine residues located near the nanopore constriction provides the required molecular recognition, thus playing a major role in the sensor sensitivity and selectivity. Although DTPMPA can interact with many metal ions, its larger binding affinity with Fe³⁺ makes the nanopore sensor more selective to the target analyte. Furthermore, the additional histidine residues near the *cis* entrance of the pore not only allow the convenient differentiation between Fe³⁺ and other metal ions such as Cu²⁺, Ni²⁺, Co²⁺, Mn²⁺, and Zn²⁺, but also enable potential simultaneous multi-metal ion detection. Our developed nanopore sensor may find useful

applications in detection of Fe³⁺ ions in body fluids and natural water for iron-related disease

prevention & diagnosis as well as environmental monitoring. In addition, the probe-assisted multi-

functionalized nanopore sensing strategy developed in this work should find useful application in

the development of stochastic sensors for a variety of other substances, especially in situations

where it is difficult to find highly selective probe molecules for the target analyte or multi-analyte

simultaneous detection is desired.

ASSOCIATE CONTENT

AUTHOR INFORMATION

Corresponding author

E-mail: xgpc2@missouri.edu

Email: wangliang83@cigit.ac.cn

Notes

The authors declare no competing financial interests.

CRediT authorship contribution statement

Pearl Arora: Conceptualization, Methodology, Investigation, Formal analysis, Data curation,

Writing – original draft. Haiyan Zheng: Investigation, Formal analysis, Data curation.

SathishKumar Munusamy: Investigation. Rana Jahani: Investigation. Liang Wang: Project

administration, Writing – review & editing. Xiyun Guan: Conceptualization, Supervision, Project

administration, Funding acquisition, Writing – review & editing.

Declaration of competing interest

16

The authors declare that they have no known competing financial interests or personal relationships that could have appeared to influence the work reported in this paper.

Acknowledgments

This work was financially supported by the National Institutes of Health (R01GM147247) and National Science Foundation (2203763 and 2345813). L. Wang appreciates the financial support from the National Key Research and Development Program of China (2022YFB3205600).

References

- Ahmad, M., Ha, J.-H., Mayse, L.A., Presti, M.F., Wolfe, A.J., Moody, K.J., Loh, S.N., Movileanu, L., 2023. A generalizable nanopore sensor for highly specific protein detection at single-molecule precision. Nat. Commun. 14, 1374. https://doi.org/10.1038/s41467-023-36944-9
- Bansod, B., Kumar, T., Thakur, R., Rana, S., Singh, I., 2017. A review on various electrochemical techniques for heavy metal ions detection with different sensing platforms. Biosens. Bioelectron. 94, 443–455. https://doi.org/10.1016/j.bios.2017.03.031
- Bayley, H., Braha, O., Gu, L.-Q., 2000. Stochastic Sensing with Protein Pores. Adv. Mater. 12, 139–142. https://doi.org/10.1002/(SICI)1521-4095(200001)12:2<139::AID-ADMA139>3.0.CO;2-Q
- Boldt, D.H., 1999. New perspectives on iron: an introduction. Am. J. Med. Sci. 318, 207–212. https://doi.org/10.1097/00000441-199910000-00001
- Cao, J., Jia, W., Zhang, J., Xu, X., Yan, S., Wang, Y., Zhang, P., Chen, H.-Y., Huang, S., 2019. Giant single molecule chemistry events observed from a tetrachloroaurate(III) embedded Mycobacterium smegmatis porin A nanopore. Nat. Commun. 10, 5668. https://doi.org/10.1038/s41467-019-13677-2
- Chakraborty, S., Mandal, M., Rayalu, S., 2020. Detection of iron (III) by chemo and fluoro-sensing technology. Inorg. Chem. Commun. 121, 108189. https://doi.org/10.1016/j.inoche.2020.108189
- Chen, K., Jou, I., Ermann, N., Muthukumar, M., Keyser, U.F., Bell, N.A.W., 2021. Dynamics of driven polymer transport through a nanopore. Nat. Phys. 17, 1043–1049. https://doi.org/10.1038/s41567-021-01268-2
- Chen, X., M. Roozbahani, G., Ye, Z., Zhang, Y., Ma, R., Xiang, J., Guan, X., 2018. Label-Free Detection of DNA Mutations by Nanopore Analysis. ACS Appl. Mater. Interfaces 10, 11519–11528. https://doi.org/10.1021/acsami.7b19774
- Chen, X., Zhang, Y., Arora, P., Guan, X., 2021. Nanopore Stochastic Sensing Based on Non-covalent Interactions. Anal. Chem. 93, 10974–10981. https://doi.org/10.1021/acs.analchem.1c02102
- Choi, L.-S., Mach, T., Bayley, H., 2013. Rates and stoichiometries of metal ion probes of cysteine residues within ion channels. Biophys. J. 105, 356–364. https://doi.org/10.1016/j.bpj.2013.04.046
- Cui, F., Sun, J., Yang, X., Ji, J., Pi, F., Zhang, Y., Lei, H., Sun, X., 2019. Ultrasensitive fluorometric determination of iron(III) and inositol hexaphosphate in cancerous and bacterial cells by using carbon dots with bright yellow fluorescence. Analyst 144, 5010–5021. https://doi.org/10.1039/C9AN00968J

- de Zoysa, R.S.S., Krishantha, D.M.M., Zhao, Q., Gupta, J., Guan, X., 2011. Translocation of single-stranded DNA through the α-hemolysin protein nanopore in acidic solutions. Electrophoresis 32, 3034-3041. https://doi.org/10.1002/elps.201100216
- dos Santos, N.K.V., dos Santos, L., Damin, I.C.F., Vale, M.G.R., Dessuy, M.B., 2022. Multielement determination of metals in edible seeds by HR-CS GF AAS and direct analysis. J. Food Compos. Anal. 111, 104625. https://doi.org/10.1016/j.jfca.2022.104625
- Gupta, J., Zhao, Q., Wang, G., Kang, X., Guan, X., 2013. Simultaneous detection of CMPA and PMPA, hydrolytes of soman and cyclosarin nerve agents, by nanopore analysis. Sens. Actuators B Chem. 176, 625–631. https://doi.org/10.1016/j.snb.2012.10.058
- Han, Y., Zhou, S., Wang, L., Guan, X., 2015. Nanopore back titration analysis of dipicolinic acid. ELECTROPHORESIS 36, 467–470. https://doi.org/10.1002/elps.201400255
- Harigae, H., 2018. Iron metabolism and related diseases: an overview. Int. J. Hematol. 107, 5–6. https://doi.org/10.1007/s12185-017-2384-0
- Hirayama, T., Nagasawa, H., 2017. Chemical tools for detecting Fe ions. J. Clin. Biochem. Nutr. 60, 39–48. https://doi.org/10.3164/jcbn.16-70
- Hu, Z.-L., Huo, M.-Z., Ying, Y.-L., Long, Y.-T., 2021. Biological Nanopore Approach for Single-Molecule Protein Sequencing. Angew. Chem. 133, 14862–14873. https://doi.org/10.1002/ange.202013462
- Kececi, K., Kaya, D., Martin, C.R., 2022. Resistive-pulse Sensing of DNA with a Polymeric Nanopore Sensor and Characterization of DNA Translocation. ChemNanoMat 8, e202100424. https://doi.org/10.1002/cnma.202100424
- Laglera, L.M., Monticelli, D., 2017. Iron detection and speciation in natural waters by electrochemical techniques: A critical review. Curr. Opin. Electrochem. 3, 123–129. https://doi.org/10.1016/j.coelec.2017.07.007
- Lee, D.-H., Oh, S., Lim, K., Lee, B., Yi, G.-S., Kim, Y.-R., Kim, K.-B., Lee, C.-K., Chi, S.-W., Lee, M.-K., 2021. Tertiary RNA Folding-Targeted Drug Screening Strategy Using a Protein Nanopore. Anal. Chem. 93, 2811–2819. https://doi.org/10.1021/acs.analchem.0c03941
- Li, X., Song, G., Dou, L., Yan, S., Zhang, M., Yuan, W., Lai, S., Jiang, X., Li, K., Sun, K., Zhao, C., Geng, J., 2021. The structure and unzipping behavior of dumbbell and hairpin DNA revealed by real-time nanopore sensing. Nanoscale 13, 11827–11835. https://doi.org/10.1039/D0NR08729G
- Liu, G., Zhang, L., Dong, D., Liu, Y., Li, J., 2016. A label-free DNAzyme-based nanopore biosensor for highly sensitive and selective lead ion detection. Anal. Methods 8, 7040–7046. https://doi.org/10.1039/C6AY02240E
- Liu, Z., Li, N., Liu, P., Qin, Z., Jiao, T., 2022. Highly Sensitive Detection of Iron Ions in Aqueous Solutions Using Fluorescent Chitosan Nanoparticles Functionalized by Rhodamine B. ACS Omega 7, 5570–5577. https://doi.org/10.1021/acsomega.1c07071
- Lu, B., Fleming, S., Szalay, T., Golovchenko, J., 2015. Thermal Motion of DNA in an MspA Pore. Biophys. J. 109, 1439–1445. https://doi.org/10.1016/j.bpj.2015.08.019
- Mady, M.F., Abdel-Azeim, S., Kelland, M.A., 2021. Antiscaling Evaluation and Quantum Chemical Studies of Nitrogen-Free Organophosphorus Compounds for Oilfield Scale Management. Ind. Eng. Chem. Res. 60, 12175–12188. https://doi.org/10.1021/acs.iecr.1c02441
- Minicozzi, V., Stellato, F., Comai, M., Dalla Serra, M., Potrich, C., Meyer-Klaucke, W., Morante, S., 2008. Identifying the minimal copper- and zinc-binding site sequence in amyloid-beta peptides. J. Biol. Chem. 283, 10784–10792. https://doi.org/10.1074/jbc.M707109200
- MohammadiRoozbahani, G., Zhang, Y., Chen, X., HoseiniSoflaee, M., Guan, X., 2019. Enzymatic-reaction Based Nanopore Detection of Zinc Ions. The Analyst 144, 7432–7436. https://doi.org/10.1039/c9an01784d

- Montal, M., Mueller, P., 1972. Formation of bimolecular membranes from lipid monolayers and a study of their electrical properties. Proc. Natl. Acad. Sci. U. S. A. 69, 3561–3566. https://doi.org/10.1073/pnas.69.12.3561
- Paz-Rodríguez, B., Domínguez-González, M.R., Aboal-Somoza, M., Bermejo-Barrera, P., 2015. Application of High Resolution-Continuum Source Flame Atomic Absorption Spectrometry (HR-CS FAAS): Determination of trace elements in tea and tisanes. Food Chem. 170, 492–500. https://doi.org/10.1016/j.foodchem.2014.08.003
- Qin, J., Su, Z., Mao, Y., Liu, C., Qi, B., Fang, G., Wang, S., 2021. Carboxyl-functionalized hollow polymer microspheres for detection of trace metal elements in complex food matrixes by ICP-MS assisted with solid-phase extraction. Ecotoxicol. Environ. Saf. 208, 111729. https://doi.org/10.1016/j.ecoenv.2020.111729
- Roozbahani, G.M., Chen, X., Zhang, Y., Juarez, O., Li, D., Guan, X., 2018. Computation-Assisted Nanopore Detection of Thorium Ions. Anal. Chem. 90, 5938–5944. https://doi.org/10.1021/acs.analchem.8b00848
- Roozbahani, G.M., Chen, X., Zhang, Y., Wang, L., Guan, X., 2020. Nanopore Detection of Metal Ions: Current Status and Future Directions. Small Methods 4, 2000266. https://doi.org/10.1002/smtd.202000266
- Roozbahani, G.M., Chen, X., Zhang, Y., Xie, R., Ma, R., Li, D., Li, H., Guan, X., 2017. Peptide-Mediated Nanopore Detection of Uranyl Ions in Aqueous Media. ACS Sens. 2, 703–709. https://doi.org/10.1021/acssensors.7b00210
- Rozevsky, Y., Gilboa, T., van Kooten, X.F., Kobelt, D., Huttner, D., Stein, U., Meller, A., 2020.

 Quantification of mRNA Expression Using Single-Molecule Nanopore Sensing. ACS Nano 14, 13964–13974. https://doi.org/10.1021/acsnano.0c06375
- Shariff, R., Aachary, A.A., Pacquette, L.H., Mittal, A.K., Girdhar, R., 2018. Analytical Method Validation and Determination of Iron and Phosphorus in Vegetable Oil by Inductively Coupled Plasma—Mass Spectrometry with Microwave Assisted Digestion. Anal. Lett. 51, 1774–1788. https://doi.org/10.1080/00032719.2017.1387554
- Shellaiah, M., Thirumalaivasan, N., Aazaad, B., Awasthi, K., Sun, K.W., Wu, S.-P., Lin, M.-C., Ohta, N., 2020. Novel rhodamine probe for colorimetric and fluorescent detection of Fe3+ ions in aqueous media with cellular imaging. Spectrochim. Acta. A. Mol. Biomol. Spectrosc. 242, 118757. https://doi.org/10.1016/j.saa.2020.118757
- Singh, S.L., Chauhan, K., Bharadwaj, A.S., Kishore, V., Laux, P., Luch, A., Singh, A.V., 2023. Polymer Translocation and Nanopore Sequencing: A Review of Advances and Challenges. Int. J. Mol. Sci. 24, 6153. https://doi.org/10.3390/ijms24076153
- Song, L., Hobaugh, M.R., Shustak, C., Cheley, S., Bayley, H., Gouaux, J.E., 1996. Structure of staphylococcal alpha-hemolysin, a heptameric transmembrane pore. Science 274, 1859–1866. https://doi.org/10.1126/science.274.5294.1859
- Song, X.-T., Yin, Y.-D., Wu, G.-R., Xu, M., Gu, Z.-Y., 2023. Nanopore-Based Metal Ion Detection and Metal Ion-Mediated Nanopore Sensing†. Chin. J. Chem. 41, 2746–2757. https://doi.org/10.1002/cjoc.202300211
- Vaneev, A.N., Timoshenko, R.V., Gorelkin, P.V., Klyachko, N.L., Erofeev, A.S., 2023. Recent Advances in Nanopore Technology for Copper Detection and Their Potential Applications. Nanomaterials 13, 1573. https://doi.org/10.3390/nano13091573
- Wang, G., Wang, L., Han, Y., Zhou, S., Guan, X., 2014. Nanopore detection of copper ions using a polyhistidine probe. Biosens. Bioelectron. 53, 453–458. https://doi.org/10.1016/j.bios.2013.10.013
- Wang, G., Zhao, Q., Kang, X., Guan, X., 2013. Probing Mercury(II)—DNA Interactions by Nanopore Stochastic Sensing. J. Phys. Chem. B 117, 4763–4769. https://doi.org/10.1021/jp309541h

- Wang, H.-Y., Song, Z.-Y., Zhang, H.-S., Chen, S.-P., 2016. Single-molecule analysis of lead(II)-binding aptamer conformational changes in an α-hemolysin nanopore, and sensitive detection of lead(II). Microchim. Acta 183, 1003–1010. https://doi.org/10.1007/s00604-015-1699-x
- Wang, L., Chen, X., Zhou, S., Roozbahani, G.M., Zhang, Y., Wang, D., Guan, X., 2018. Displacement chemistry-based nanopore analysis of nucleic acids in complicated matrices. Chem. Commun. 54, 13977–13980. https://doi.org/10.1039/C8CC07944G
- Wang, L., Han, Y., Zhou, S., Wang, G., Guan, X., 2014. Nanopore Biosensor for Label-Free and Real-Time Detection of Anthrax Lethal Factor. ACS Appl. Mater. Interfaces 6, 7334–7339. https://doi.org/10.1021/am500749p
- Wang, L., Yao, F., Kang, X., 2017. Nanopore Single-Molecule Analysis of Metal Ion–Chelator Chemical Reaction. Anal. Chem. 89, 7958–7965. https://doi.org/10.1021/acs.analchem.7b01119
- Wang, S., Cao, J., Jia, W., Guo, W., Yan, S., Wang, Y., Zhang, P., Chen, H.-Y., Huang, S., 2020. Single molecule observation of hard–soft-acid–base (HSAB) interaction in engineered Mycobacterium smegmatis porin A (MspA) nanopores. Chem. Sci. 11, 879–887. https://doi.org/10.1039/C9SC05260G
- Wanunu, M., Morrison, W., Rabin, Y., Grosberg, A.Y., Meller, A., 2010. Electrostatic focusing of unlabelled DNA into nanoscale pores using a salt gradient. Nat. Nanotechnol. 5, 160–165. https://doi.org/10.1038/nnano.2009.379
- Wei, K., Yao, F., Kang, X.-F., 2018. Single-molecule porphyrin-metal ion interaction and sensing application. Biosens. Bioelectron. 109, 272–278. https://doi.org/10.1016/j.bios.2018.03.002
- Wu, X., Xi, J., Wei, X., Yin, C., 2023. An ultra-fast UV-electrochemical sensor based on Cu-MOF for highly sensitive and selective detection of ferric ions. Analyst 148, 366–373. https://doi.org/10.1039/D2AN01865A
- Ye, S., Zhang, M., Guo, J., Song, J., Zeng, P., Qu, J., Chen, Y., Li, H., 2022. Facile Synthesis of Green Fluorescent Carbon Dots and Their Application to Fe3+ Detection in Aqueous Solutions. Nanomaterials 12, 1487. https://doi.org/10.3390/nano12091487
- Yu, X., He, M., Chen, B., Hu, B., 2020. Recent advances in single-cell analysis by inductively coupled plasma-mass spectrometry: A review. Anal. Chim. Acta 1137, 191–207. https://doi.org/10.1016/j.aca.2020.07.041
- Zhan, K., Li, Z., Chen, J., Hou, Y., Zhang, J., Sun, R., Bu, Z., Wang, L., Wang, M., Chen, X., Hou, X., 2020. Tannic acid modified single nanopore with multivalent metal ions recognition and ultra-trace level detection. Nano Today 33, 100868. https://doi.org/10.1016/j.nantod.2020.100868
- Zhang, Y., Chen, X., Wang, C., Chang, H.-C., Guan, X., 2022. Nanoparticle-assisted detection of nucleic acids in a polymeric nanopore with a large pore size. Biosens. Bioelectron. 196, 113697. https://doi.org/10.1016/j.bios.2021.113697
- Zhang, Y., Chen, X., Wang, C., Roozbahani, G.M., Chang, H.-C., Guan, X., 2020. Chemically functionalized conical PET nanopore for protein detection at the single-molecule level. Biosens. Bioelectron. 165, 112289. https://doi.org/10.1016/j.bios.2020.112289
- Zhao, Q., Jayawardhana, D.A., Guan, X., 2008. Stochastic Study of the Effect of Ionic Strength on Noncovalent Interactions in Protein Pores. Biophys. J. 94, 1267–1275. https://doi.org/10.1529/biophysj.107.117598
- Zhou, S., Wang, L., Chen, X., Guan, X., 2016. Label-free nanopore single-molecule measurement of trypsin activity. ACS Sens. 1, 607–613. https://doi.org/10.1021/acssensors.6b00043
- Zhu, Y., Pan, D., Hu, X., Han, H., Lin, M., Wang, C., 2017. An electrochemical sensor based on reduced graphene oxide/gold nanoparticles modified electrode for determination of iron in coastal waters. Sens. Actuators B Chem. 243, 1–7. https://doi.org/10.1016/j.snb.2016.11.108